GEOLOGY | THE GEOLOGICAL SOCIETY OF AMERICA®

https://doi.org/10.1130/G45329.1

Manuscript received 30 June 2018
Revised manuscript received 18 September 2018
Manuscript accepted 23 September 2018

Published online 12 October 2018

Perovskite U-Pb and Sr-Nd isotopic perspectives on melilitite magmatism and outward growth of the Tibetan Plateau

Dong Liu[1]*, Zhidan Zhao[1], Yaoling Niu[1,2], Di-Cheng Zhu[1], and Xian-Hua Li[3]

[1]State Key Laboratory of Geological Processes and Mineral Resources, and School of Earth Science and Resources, China University of Geosciences, Beijing 100083, China

[2]Department of Earth Sciences, Durham University, Durham DH1 3LE, UK

[3]State Key Laboratory of Lithospheric Evolution, Institute of Geology and Geophysics, Chinese Academy of Sciences, Beijing 100029, China

ABSTRACT

Mantle-derived alkaline magmatism along major strike-slip faults provides unique insights into the lateral growth of the Tibetan Plateau. Here we use the geochemistry of perovskites from the West Qinling melilitite to probe into the nature and dynamics of sub-lithospheric mantle beneath the northeastern Tibetan Plateau. The texture and chemical composition of perovskites indicate their early crystallization from a CO_2-rich melilitite magma. Most perovskite crystals have moderately depleted Sr-Nd isotopic compositions, whereas a few grains exhibit high $^{87}Sr/^{86}Sr_i$ and low $\varepsilon_{Nd}(t)$. Together with the bulk-rock geochemistry of the melilitite, the perovskite Sr-Nd isotope data imply that the primary magma parental to the melilitite was most likely derived from seafloor subduction–modified asthenosphere and underwent interaction with lithospheric mantle during ascent. *In situ* U-Pb dating of the perovskites demonstrates the temporal correlation between the melilitite magmatism and Kunlun strike-slip faulting in the early Miocene. These findings indicate the fundamental role of India-Asia convergence in driving outward plateau growth through strike-slip extrusion and in reactivating long-lived lithospheric zones of weakness for evacuating low-volume asthenospheric melts.

INTRODUCTION

The outward growth and strike-slip extrusion of the Tibetan Plateau are accompanied by low-volume and deeply rooted alkaline magmatism (e.g., Wang et al., 2001; Mahéo et al., 2009; Dai et al., 2017). The resulting alkaline rocks can offer valuable insights into mantle dynamics (Molnar et al., 1993; Tapponnier et al., 2001) and allow a better understanding of the tectonic and topographic evolution of the India-Asia collision zone (see the review by Wang et al. [2014]). However, inevitable contamination and hydrothermal alteration at crustal levels make it difficult to constrain the nature of sources through bulk-rock data from mantle-derived rocks (Tappe et al., 2012; Sun et al., 2014). The lack of accurate and precise age data on alkaline rocks with mantle affinity also leads to ambiguities in their correlations with regional tectonic processes on various scales and hampers understanding how the Tibetan Plateau may have grown laterally in space and time.

Perovskite ($CaTiO_3$) is a common accessory mineral in SiO_2-undersaturated rocks and serves as a major carrier of Th, U, Sr, and rare earth elements (Chakhmouradian et al., 2013). It is thus suitable for U-Th-Pb dating, and its radiogenic isotopes can also provide reliable information about magmatic sources and processes (Yang et al., 2009; Tappe et al., 2012). Here we present a combined study of *in situ* U-Pb dating, trace element analysis, and Sr-Nd isotope compositions on perovskites extracted from melilitite samples in the West Qinling orogenic belt. These data, together with seismic tomography across the Kunlun fault zone, provide new perspectives on the geochemical and dynamic evolution of upper mantle beneath the northeastern Tibetan Plateau. This study also presents the first perovskite U-Pb ages for melilitite magmatism on the greater Tibetan Plateau, which highlight the critical role of translithospheric lineaments in the generation and emplacement of postcollisional alkaline magmatism and illustrate a detailed pattern for outward plateau growth.

TECTONIC SETTING AND SAMPLE DESCRIPTIONS

The Qinling orogenic belt stretches eastward through the Dabie orogen, connects with the Kunlun orogen to the west, and preserves numerous metamorphic and magmatic records of Proterozoic–Mesozoic seafloor subduction and continental collision episodes (Dong and Santosh, 2016). The western part of the Qinling orogenic belt is a conjunction region of the Tibetan Plateau and the North and South China blocks (Fig. 1A). In the Cenozoic, the northeastern Tibetan Plateau underwent significant lithospheric deformation and tectonic rotation and developed numerous thrust and strike-slip faults to accommodate the continued India-Asia convergence (Tapponnier et al., 2001; Wang et al., 2014). The Kunlun fault (>1500 km long) is a prominent left-lateral strike-slip fault zone in northern and northeastern Tibet. It propagates along the plate boundary between the Songpan-Ganzi-Hohxil terrane and eastern Kunlun and extends eastward into the West Qinling orogenic belt (Fig. 1A). A thermochronological study on the exhumation history associated with Kunlun strike-slip faulting indicates that this sinistral fault may have initiated in the early Miocene or earlier (20–15 Ma) with a total offset of 100–300 km and a high Quaternary slip rate (≥10 mm/yr) (Duvall et al., 2013).

Postcollisional (ultra)potassic volcanic centers in the Songpan-Ganzi-Hohxil terrane are scattered along the west segment of Kunlun fault (Fig. 1A), providing K-Ar and Ar-Ar ages ranging from 24.6 Ma to 0.30 Ma (Table DR1 in the GSA Data Repository[1]). To the east, several rhomb-shaped Cenozoic basins have developed along and adjacent to the Kunlun fault. The West Qinling melilitite, which commonly occurs as volcanic pipes and lavas, is distributed in the Lixian Basin (Fig. DR1 in the Data Repository). Mantle xenoliths and carbonate ocelli

*E-mail: d.liu@cugb.edu.cn

CITATION: Liu, D., et al., 2018, Perovskite U-Pb and Sr-Nd isotopic perspectives on melilitite magmatism and outward growth of the Tibetan Plateau: Geology, v. 46, p. 1027–1030, https://doi.org/10.1130/G45329.1

[1]GSA Data Repository item 2018391, methods and analytical results (Tables DR1–DR8 and Figs. DR1–DR7), is available online at http://www.geosociety.org/datarepository/2018/ or on request from editing@geosociety.org.

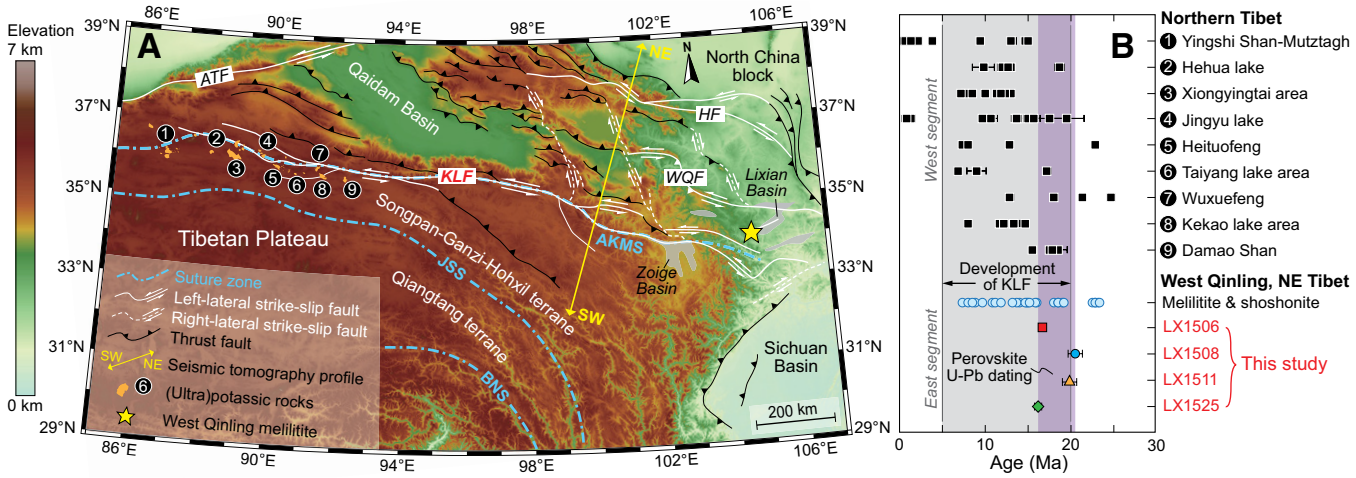

Figure 1. A: Topographic map of northeastern Tibetan Plateau, showing tectonic framework and spatial distribution of postcollisional magmatism along Kunlun fault. AKMS—Ayimaqin-Kunlun-Mutztagh suture zone; JSS—Jinsha suture zone; BNS—Bangong-Nujiang suture zone; ATF—Altyn Tagh fault; HF—Haiyuan fault; KLF—Kunlun fault; WQF—West Qinling fault. Cenozoic basins in northeastern Tibet are denoted by gray areas. Yellow line corresponds to profiles in Figure 4. B: Variation in formation ages of melilitite, shoshonite, and (ultra)potassic rocks along Kunlun fault (summarized in Table DR1 [see footnote 1]).

can be identified from melilititic lava, and, in some areas, melilititic lava is interbedded with extrusive Ca-carbonatites (Fig. DR2). Melilitite samples have a porphyritic texture with phenocrysts dominated by pyroxenes, olivine, and minor phlogopite in a fine-grained groundmass. Their groundmass mineralogy includes melilite, nepheline, leucite, perovskite, and Fe-Ti oxides. The melilitites and shoshonites in West Qinling yield K-Ar and Ar-Ar eruption ages of 23.2–8.7 Ma (Table DR1 and references therein).

METHODS AND RESULTS

Bulk-rock major and trace element compositions of melilitite samples were measured at China University of Geosciences (Wuhan). Perovskites extracted from the melilitite were mounted in epoxy resin and selected for *in situ* analyses at the Institute of Geology and Geophysics, Chinese Academy of Sciences. Analytical methods and results are given in the Data Repository.

The West Qinling melilitite is a suite of SiO_2-undersaturated volcanic rocks with low Al_2O_3 (as low as 7.65 wt%), high MgO (12.7–18.5 wt%), and high CaO (up to 14.2 wt%) contents (Table DR2). They have low K_2O/Na_2O (0.5–1) and plot in the compositional fields of melilitite and nephelinite (Fig. DR3). The primitive mantle–normalized trace element patterns of the melilitite samples are characterized by relative enrichment of large ion lithophile elements (LILEs) and light rare earth elements (LREEs), with weak negative anomalies in Rb, Zr, Hf, and Ti (Fig. DR3).

Perovskites from the melilitite commonly grow as euhedral and subhedral grains of varying size (50–200 μm). They are homogeneous and do not show oscillatory zoning in backscattered electron (BSE) images (Fig. DR4). Mineral inclusions are rare, and alterations are not observed in these unzoned grains. The analyzed grains are almost pure $CaTiO_3$ (91.3–97.6 mol%) with minor SiO_2 (<0.17 wt%) and Na_2O (0.21–1.35 wt%) (Table DR3). All grains exhibit negative Rb, Ba, Pb, Sr, Zr, Hf, and Y anomalies, showing elevated LREEs relative to heavy rare earth elements (HREEs) (Fig. 2).

Perovskites have varying Th (10.3–1462 ppm) and U (50.8–333 ppm) contents and a wide range of Th/U (0.09–23.6; Tables DR3 and DR4). The isotopic data for each sample define an array that intercepts the inverse concordia curve in the Tera-Wasserburg diagram and yields lower-intercept ages ranging from 15.93 ± 0.44 Ma to 20.06 ± 0.84 Ma (Fig. DR5). The weighted mean $^{206}Pb/^{238}U$ age based on the ^{207}Pb-correction method vary from 16.19 ± 0.42 Ma to 20.35 ± 0.89 Ma, which agrees well with lower-intercept ages for each sample.

Unradiogenic Sr and radiogenic Nd isotopic compositions can be observed in melilititic perovskites (Fig. 3). Except for a few grains (e.g., grain LX1506@12; Tables DR5 and DR6), the initial Sr isotopic ratios in perovskites ($^{87}Sr/^{86}Sr_i$ = 0.7026–0.7042) are lower than the bulk-rock values of the host melilitite ($^{87}Sr/^{86}Sr_i$ = 0.7037–0.7094) and mantle xenoliths ($^{87}Sr/^{86}Sr_i$ = 0.7040–0.7056). Both perovskites [$\varepsilon_{Nd}(t)$ = +0.1 to +7.5] and mantle xenoliths [$\varepsilon_{Nd}(t)$ = +1.3 to +7.1] have a narrower range in initial Nd isotopic variations than the melilitite [$\varepsilon_{Nd}(t)$ = –4.6 to +6.1].

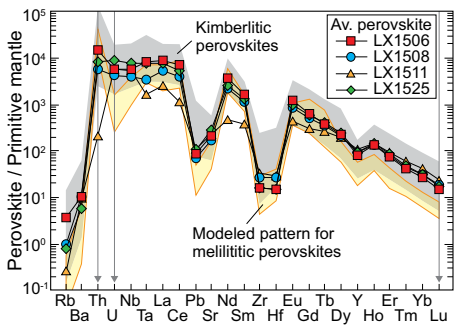

Figure 2. Primitive mantle (values from Sun and McDonough, 1989)–normalized diagram, illustrating average trace element compositions of perovskites from each sample. Field of kimberlitic perovskites (Yang et al., 2009; Sun et al., 2014) is shown for comparison. The modeled pattern is calculated through bulk-rock data of the melilitite.

DISCUSSION

Textural and Trace Element Constraints on the Origin of Perovskite

Perovskite is an early-crystallizing phase in SiO_2-undersaturated rocks, and its textural appearance and chemical composition may reflect the nature of primary magmas and rock-forming processes (Yang et al., 2009; Chakhmouradian et al., 2013). Texturally, the groundmass perovskites from the melilitite are euhedral to subhedral and show uniform and smooth appearance in BSE images (Fig. DR4), which apparently differ from altered grains with spongy appearance (Yang et al., 2009). The homogeneous internal texture and the lack of late-crystallizing mineral inclusions (e.g., calcite and mica) also indicate that these unaltered perovskites were formed in the early stage of crystallization.

Geochemical compositions of the melilititic perovskites provide further evidence for their primary magmatic origin (Fig. 2). The studied perovskites commonly have low SiO_2 and high CaO contents (Table DR3), which are in contrast with those grains altered by post-crystallization hydrothermal events and preclude the occurrence of secondary alteration and/or modification (Yang et al., 2009). Moreover, perovskites from the West Qinling melilitite show compositional similarity to those from kimberlites worldwide (Fig. 2). Experimental studies have shown that

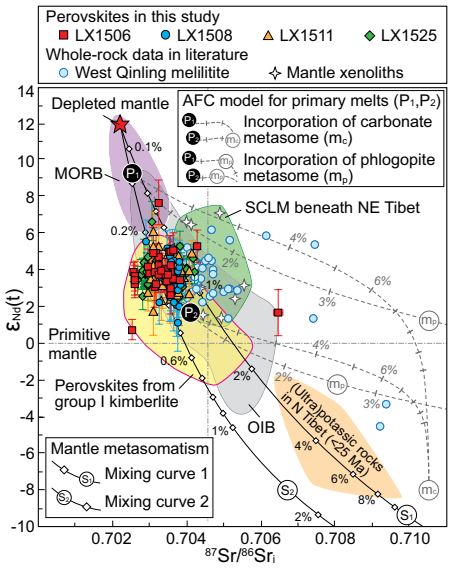

Figure 3. Initial Sr-Nd isotopic compositions of perovskites, West Qinling melilitite, and mantle xenoliths. Labeled percentages along assimilation and fractional crystallization (AFC) modeling and binary mixing curves denote increments of subcontinental lithospheric mantle (SCLM) contaminants and recycled sediments, respectively. Partition coefficients D_{Sr} (0.6) and D_{Nd} (0.2) were estimated by assuming cumulates of pyroxene + plagioclase + olivine + phlogopite + perovskite, and *R* value was set to be 0.99. Details of end-members used in geochemical modeling are given in Table DR8 (see footnote 1). Fields of mid-oceanic ridge basalt (MORB) and ocean island basalt (OIB) (http://georoc.mpch-mainz.gwdg.de/georoc/), kimberlitic perovskites (Tappe et al., 2012; Sun et al., 2014), SCLM beneath northeastern Tibet (Su et al., 2012), and (ultra) potassic rocks in northern Tibet (Guo et al., 2006) are shown for comparison.

trace element systematics of perovskite is mainly controlled by melt composition and substitution mechanisms rather than pressure and temperature (Beyer et al., 2013; Chakhmouradian et al., 2013). We thus modeled their trace element compositions using bulk-rock data of melilitite samples and partition coefficients ($D_{element}$) with katungite (i.e., potassic olivine melilitite; Chakhmouradian et al., 2013). The modeling indicates that the distinctive signatures of the studied perovskites, including the enrichment of LREEs and relative deletions in Rb, Ba, Pb, Sr, Zr, and Hf, can be well reproduced by equilibrium crystallization from a melilitite parental magma (Fig. 2).

We also note that the melilititic perovskites display variably lower Th/U and higher HREEs concentrations than the modeled trace element pattern (Fig. 2). Growth in a primary magma with higher concentrations of U and HREEs cannot fully explain the difference between measured and calculated results, because perovskite has a strong preference for Th (D_{Th} = 155) and LREEs (D_{La} = 27.9) and exhibits high D_{Th}/D_{U} (up to 23) and D_{La}/D_{Lu} (up to 14.7) during crystallization from katungite magma (Chakhmouradian et al., 2013). A likely explanation is that the perovskite-melilitite trace element partitioning was affected by melt structure. Compared with a pure silicate magmatic system, perovskite crystallizing from a carbonatite or a hybrid carbonate-silicate magma would have much lower D_{Th}/D_{U} (0.57–9.23) and D_{La}/D_{Lu} (0.68–6.25) (Beyer et al., 2013). The low Th/U and La/Yb in the analyzed perovskites thus argue for crystallization from a CO_2-rich primitive melilitite magma.

Perovskite Sr-Nd Isotopic Insights into the Petrogenesis of West Qinling Melilitite

The early-crystallizing perovskites can better preserve isotopic signatures of the primary magma than the bulk-rock samples (Tappe et al., 2012; Sun et al., 2014). *In situ* Sr-Nd isotopic analyses indicate that most perovskites display lower $^{87}Sr/^{86}Sr_i$ and slightly higher $\varepsilon_{Nd}(t)$ than the melilitite and entrained mantle xenoliths (Fig. 3). The Sr-Nd isotopic variation in mantle-derived rocks may result from source heterogeneities or reflect contamination and/or alteration during magmatic ascent and eruption. The entrainment of various peridotite xenoliths provides convincing evidence for the incorporation of mantle materials into the melilitite magma during ascent through the subcontinental lithospheric mantle (SCLM) (Su et al., 2012). We modeled the possible assimilation and fractional crystallization (AFC) processes and found that the scatter of bulk-rock Sr-Nd isotopes in melilitites, as well as their isotopic overlap with mantle xenoliths, can be fully reproduced by incorporating isotopically enriched components from the SCLM (e.g., carbonate- and phlogopite-rich metasomes) into primary melts (Fig. 3). In this case, the high $^{87}Sr/^{86}Sr_i$ and low $\varepsilon_{Nd}(t)$ observed in some perovskite grains (e.g., grain LX1506@12) can be best explained as reflecting the chemical interaction between the primary melilitite magma and the metasomatized SCLM. The discrepancy between *in situ* perovskite data and bulk-rock isotopic compositions thus underscores the potential of early-crystallizing perovskites for probing into the nature of mantle sources and also corroborates the inevitable lithospheric contamination of primary melilitite magma during its ascent.

A common characteristic of perovskites from the West Qinling melilitite and from group I kimberlites worldwide is their comparable Sr-Nd isotopic covariations that overlap with the variation range of modern ocean island basalt (OIB) and form arrays extending toward the isotopic composition of depleted mantle (Fig. 3). Hence both the heterogeneous SCLM and depleted mantle asthenosphere are possible source regions for generating the primary melilitite magma. However, the entrained mantle xenoliths permit direct insights into the SCLM beneath the northeastern Tibetan Plateau (Su et al., 2012). The pronounced difference in Pb isotopic compositions between the melilitite ($^{206}Pb/^{204}Pb$ = 18.088–19.441) and mantle xenoliths ($^{206}Pb/^{204}Pb$ = 16.083–18.020) (Fig. DR6) argues against a derivation from partial melting of the SCLM. Melting within mantle lithosphere is further challenged by a thermobarometric calculation performed on peridotite xenoliths because it gives their depths of origin as greater as 65–125 km (Su et al., 2012) and limits the minimum depth at which mantle melting and extraction of incipient melilitite melts have occurred. With respect to the lithospheric thickness beneath the northeastern Tibetan Plateau (100–130 km; Li et al., 2013), the primary melilitite magma should originate at a depth greater than that of the lithosphere-asthenosphere boundary (LAB).

Considering the Permian–Triassic northward subduction of the Ayimaqin-Kunlun-Mianlue Paleo-Tethyan oceanic lithosphere beneath the West Qinling orogenic belt (cf. Dong and Santosh, 2016), we propose that the primary melilitite magma was ultimately derived from low-degree partial melting of the subduction-modified asthenosphere. We find that addition of minor amounts (<1%) of carbonate-bearing pelagic sediments to the depleted mantle is sufficient to reproduce the Sr-Nd isotopic array defined by the melilititic perovskites (Fig. 3). Such interpretation is compatible with the OIB-like trace element features (e.g., high Ce/Pb and Nb/U; Fig. DR3) and the radiogenic Pb isotopic compositions (Fig. DR6) shown by the West Qinling melilitite. It is also supported by experimental results in which melilitite melts are generated via small-degree (<1%) melting of CO_2-bearing peridotite (<4 GPa; Gudfinnsson and Presnall, 2005), particularly if the isotopically light Mg in the melilitite ($\delta^{26}Mg$ = –0.54‰ to –0.32‰; Dai et al., 2017) is considered to represent carbonate-related metasomatism in mantle sources. When considered in conjunction with Neogene–Quaternary (ultra)potassic magmatism in northern Tibet (Guo et al., 2006), it is tenable that multiple episodes of oceanic subduction and continental convergence could have resulted in significant heterogeneities in the upper mantle and consequently contributed to postcollisional alkaline magmatism along the Kunlun fault zone.

Implications for the Northeastward Growth of the Tibetan Plateau

Identification of mantle-derived alkaline magmatism and how it relates to tectonic escape in response to the India-Asia convergence are key to unraveling the outward-growth mechanism of the Tibetan Plateau (Tapponnier et al., 2001; Wang et al., 2001). Our new perovskite U-Pb ages indicate that the melilitite magmatism is broadly coeval with (ultra)potassic activities in northern Tibet (Fig. 1B), both of which coincide with Kunlun strike-slip faulting that began in the

early Miocene (Duvall et al., 2013). The linear distribution and long temporal span (~25 m.y.) represented by these postcollisional magmatic rocks (Fig. 1) argue against a rapid removal of the SCLM beneath northern Tibet. Because seismic tomography shows a low-velocity dome right beneath the Kunlun fault zone at a depth of 90–150 km (Fig. 4), an alternative explanation is that these small-volume alkaline rocks may be formed via decompression melting of mantle asthenosphere and emplaced along narrow conduits of the Kunlun fault zone. For the West Qinling melilitite, carbonatite metasomatism would dramatically lower the solidus temperature in mantle sources and facilitate the occurrence of mantle melting (Gudfinnsson and Presnall, 2005). Meanwhile, the deeply rooted Kunlun fault system, which propagates along the weakly welded Ayimaqin-Kunlun-Mutztagh suture zone (Fig. 1A) and cuts through the entire lithosphere (Li et al., 2013), would provide magmatic pathways and allow such volatile-rich magma to migrate rapidly to the surface.

Given that the continued India-Asia convergence would reactivate preexisting zones of weakness in the Asian lithosphere away from the collision zone (Tapponnier et al., 2001), the highly localized decompression melting of refertilized mantle asthenosphere may also explain the formation of alkaline magmatism along the Ailao Shan–Red River shear zone (Wang et al., 2001) and Karakorum-Shigar strike-slip fault zone (Mahéo et al., 2009). Therefore, our perovskite U-Pb dating results not only provide a time constraint on the initiation of Kunlun strike-slip faulting and associated tension gash, but also highlight the controlling role of preexisting lithospheric weakness in intracontinental deformation, tectonic extrusion, and emplacement of postcollisional magmatism accompanying the outward plateau growth.

CONCLUSIONS

The textural and geochemical features of perovskite crystals are consistent with their early crystallization from a CO_2-rich melilitite magma. The moderately depleted Sr-Nd isotopic signatures in these perovskites, as well as the OIB-like characteristics shown by the West Qinling melilitite, indicate that primary magma could originate from the low-degree partial melting of refertilized mantle asthenosphere. Perovskite U-Pb dating results corroborate the temporal correlation between the melilitite magmatism and Kunlun strike-slip faulting. The generation of volumetrically small mantle-derived alkaline magmatism along major strike-slip faults can be best interpreted as resulting from the partial melting of metasomatized asthenosphere induced by reactivation of translithospheric shear zones.

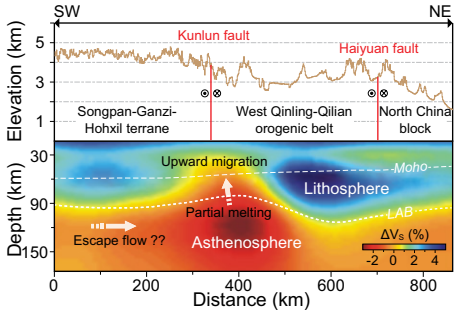

Figure 4. Topographic (top) and seismic tomography (bottom) profiles (see Fig.1 for location) across northeastern Tibet (Li et al., 2013), showing shear wave velocity (V_s) perturbation beneath Kunlun fault zone. Arrows denote possible escape flow and upward migration of asthenospheric melts along Kunlun fault system. LAB—lithosphere-asthenosphere boundary.

ACKNOWLEDGMENTS

We thank Chris Clark for editorial handling, and Jörn-Frederik Wotzlaw, Catherine Mottram, and Sebastian Tappe for insightful comments. We are grateful to Yue-Heng Yang, Qiu-Li Li, Xiao-Xiao Ling, and Qian Ma for assistance with in situ analysis. This study was supported by the China 973 Program (project 2015CB452604), the Natural Science Foundation of China (grant 41802058), and the 111 project of China (project B18048).

REFERENCES CITED

Beyer, C., Berndt, J., Tappe, S., and Klemme, S., 2013, Trace element partitioning between perovskite and kimberlite to carbonatite melt: New experimental constraints: Chemical Geology, v. 353, p. 132–139, https://doi.org/10.1016/j.chemgeo.2012.03.025.

Chakhmouradian, A.R., Reguir, E.P., Kamenetsky, V.S., Sharygin, V.V., and Golovin, A.V., 2013, Trace-element partitioning in perovskite: Implications for the geochemistry of kimberlites and other mantle-derived undersaturated rocks: Chemical Geology, v. 353, p. 112–131, https://doi.org/10.1016/j.chemgeo.2013.01.007.

Dai, L.-Q., Zhao, Z.-F., Zheng, Y.-F., An, Y.-J., and Zheng, F., 2017, Geochemical distinction between carbonate and silicate metasomatism in generating the mantle sources of alkali basalts: Journal of Petrology, v. 58, p. 863–884, https://doi.org/10.1093/petrology/egx038.

Dong, Y., and Santosh, M., 2016, Tectonic architecture and multiple orogeny of the Qinling Orogenic Belt, Central China: Gondwana Research, v. 29, p. 1–40, https://doi.org/10.1016/j.gr.2015.06.009.

Duvall, A.R., Clark, M.K., Kirby, E., Farley, K.A., Craddock, W.H., Li, C., and Yuan, D.-Y., 2013, Low-temperature thermochronometry along the Kunlun and Haiyuan Faults, NE Tibetan Plateau: Evidence for kinematic change during late-stage orogenesis: Tectonics, v. 32, p. 1190–1211, https://doi.org/10.1002/tect.20072.

Gudfinnsson, G.H., and Presnall, D.C., 2005, Continuous gradations among primary carbonatitic, kimberlitic, melilititic, basaltic, picritic, and komatiitic melts in equilibrium with garnet lherzolite at 3–8 GPa: Journal of Petrology, v. 46, p. 1645–1659, https://doi.org/10.1093/petrology/egi029.

Guo, Z., Wilson, M., Liu, J., and Mao, Q., 2006, Post-collisional, potassic and ultrapotassic magmatism of the northern Tibetan Plateau: Constraints on characteristics of the mantle source, geodynamic setting and uplift mechanisms: Journal of Petrology, v. 47, p. 1177–1220, https://doi.org/10.1093/petrology/egl007.

Li, L., Li, A., Shen, Y., Sandvol, E.A., Shi, D., Li, H., and Li, X., 2013, Shear wave structure in the northeastern Tibetan Plateau from Rayleigh wave tomography: Journal of Geophysical Research: Solid Earth, v. 118, p. 4170–4183, https://doi.org/10.1002/jgrb.50292.

Mahéo, G., Blichert-Toft, J., Pin, C., Guillot, S., and Pêcher, A., 2009, Partial melting of mantle and crustal sources beneath south Karakorum, Pakistan: Implications for the Miocene geodynamic evolution of the India-Asia convergence zone: Journal of Petrology, v. 50, p. 427–449, https://doi.org/10.1093/petrology/egp006.

Molnar, P., England, P., and Martinod, J., 1993, Mantle dynamics, uplift of the Tibetan Plateau, and the Indian monsoon: Reviews of Geophysics, v. 31, p. 357–396, https://doi.org/10.1029/93RG02030.

Su, B.-X., Zhang, H.-F., Ying, J.-F., Tang, Y.-J., Hu, Y., and Santosh, M., 2012, Metasomatized lithospheric mantle beneath the western Qinling, Central China: insight into carbonatite melts in the mantle: The Journal of Geology, v. 120, p. 671–681, https://doi.org/10.1086/667956.

Sun, J., Liu, C.-Z., Tappe, S., Kostrovitsky, S.I., Wu, F.-Y., Yakovlev, D., Yang, Y.-H., and Yang, J.-H., 2014, Repeated kimberlite magmatism beneath Yakutia and its relationship to Siberian flood volcanism: Insights from *in situ* U-Pb and Sr-Nd perovskite isotope analysis: Earth and Planetary Science Letters, v. 404, p. 283–295, https://doi.org/10.1016/j.epsl.2014.07.039.

Sun, S.S., and McDonough, W.F., 1989, Chemical and isotopic systematics of oceanic basalts: Implications for mantle composition and processes, *in* Saunders, A.D., and Norry, M.J., eds., Magmatism in the Ocean Basins: Geological Society of London Special Publication 42, p. 313–345, https://doi.org/10.1144/GSL.SP.1989.042.01.19.

Tappe, S., Steenfelt, A., and Nielsen, T., 2012, Asthenospheric source of Neoproterozoic and Mesozoic kimberlites from the North Atlantic craton, West Greenland: New high-precision U-Pb and Sr-Nd isotope data on perovskite: Chemical Geology, v. 320, p. 113–127, https://doi.org/10.1016/j.chemgeo.2012.05.026.

Tapponnier, P., Xu, Z., Roger, F., Meyer, B., Arnaud, N., Wittlinger, G., and Yang, J., 2001, Oblique stepwise rise and growth of the Tibet Plateau: Science, v. 294, p. 1671–1677, https://doi.org/10.1126/science.105978.

Wang, C., Dai, J., Zhao, X., Li, Y., Graham, S.A., He, D., Ran, B., and Meng, J., 2014, Outward-growth of the Tibetan Plateau during the Cenozoic: A review: Tectonophysics, v. 621, p. 1–43, https://doi.org/10.1016/j.tecto.2014.01.036.

Wang, J.-H., Yin, A., Harrison, T.M., Grove, M., Zhang, Y.-Q., and Xie, G.-H., 2001, A tectonic model for Cenozoic igneous activities in the eastern Indo-Asian collision zone: Earth and Planetary Science Letters, v. 188, p. 123–133, https://doi.org/10.1016/S0012-821X(01)00315-6.

Yang, Y.-H., Wu, F.-Y., Wilde, S.A., Liu, X.-M., Zhang, Y.-B., Xie, L.-W., and Yang, J.-H., 2009, *In situ* perovskite Sr-Nd isotopic constraints on the petrogenesis of the Ordovician Mengyin kimberlites in the North China Craton: Chemical Geology, v. 264, p. 24–42, https://doi.org/10.1016/j.chemgeo.2009.02.011.

Printed in USA